Biomass Conversion and Biorefinery (2024) 14:649–662
https://doi.org/10.1007/s13399-021-02279-y

ORIGINAL ARTICLE

Synthesis of activated carbon from Lemna minor plant and magnetized with iron (III) oxide magnetic nanoparticles and its application in removal of Ciprofloxacin

Murat Yilmaz[1] · Tariq J. Al-Musawi[2] · Morteza khodadadi Saloot[3] · Aram Dokht Khatibi[4] · Marziyeh Baniasadi[5] · Davoud Balarak[4]

Received: 19 October 2021 / Revised: 22 December 2021 / Accepted: 23 December 2021 / Published online: 5 January 2022

Abstract

The current study was done by preparing activated carbon from the common duckweed, Lemna minor, after magnetization using Fe_3O_4 nanoparticles. The resultant product (Fe_3O_4-ACLM) was employed to adsorb ciprofloxacin (CIP) from the contaminated water, in the batch adsorption mode. The characteristic distinctive features or parameters of the materials utilized were ascertained with the aid of scanning electron microscopy (SEM), energy–dispersive X-ray spectroscopy (EDX), Fourier transform infrared spectroscopy (FTIR), and transmission electron microscopy (TEM); the Brunauer–Emmett–Teller (BET) and Barrett–Joyner–Halenda (BJH) analysis, point of zero charge (pH_{pzc}), and vibrating sample magnetometry (VSM) were also used. From the results, it was clear that when the initial CIP concentration was 25 mg/L, and pH was 3, in the presence of Fe_3O_4-ACLM in a 0.75 g/L dosage, and contact time of 75 min, 100% removal percentage was achieved. However, the adsorbent recycling and reuse tests demonstrated that in just six periods of adsorbent use a marginal 8.5% decrease was noted in the adsorbent efficiency. The Fe_3O_4-ACLM was observed to show super-paramagnetic behavior with 37.6 emu/g saturation magnetization. Four models namely the Langmuir, Freundlich, Dubinin–Radushkevich (D-R), and Temkin isotherms were used for the adsorption isotherm studies. From the results of the goodness-of-fit parameters, the Langmuir isotherm revealed greater consistency with the equilibrium data, demonstrating maximum adsorption capacities of 134.2, 149.5, 161.4, and 178.7 mg/g at temperatures of 20, 30, 40, and 50 °C, respectively. Further, the CIP adsorption onto the Fe_3O_4-ACLM surface was, by nature, endothermic and spontaneous, according to the thermodynamic study. In conclusion, the Fe_3O_4-ACLM was proven to be efficient, recyclable, and excellent as an alternative adsorbent capable of CIP antibiotic removal from contaminated water.

Keywords Adsorption · Ciprofloxacin · Activated carbon · Fe_3O_4-ACLM · Error function

✉ Davoud Balarak
dbalarak2@gmail.com

1 Department of Chemical Engineering, Faculty of Engineering, Osmaniye Korkut Ata University, 80000 Osmaniye, Turkey

2 Building and Construction Techniques Engineering Department, Al-Mustaqbal University College, 51001 Hillah, Babylon, Iraq

3 Department of Environmental Engineering, Faculty of Natural Resources and Environment, Science and Research Branch, Islamic Azad University, Tehran, Iran

4 Department of Environmental Health, Health Promotion Research Center, Zahedan University of Medical Sciences, Zahedan, Iran

5 Student Research Committee, Zahedan University of Medical Sciences, Zahedan, Iran

1 Introduction

One alarming result of the escalating growth in the global population is the pollution of the surface and underground water, which has placed a ceiling on the demand for fresh water, with repercussions on the environment and health [1, 2]. Antibiotics rank high as the commonest and most hazardous pollutants present in pharmaceutical wastewater [3]. Reports from several research studies, over the last decade, show that the quantity of antibiotics produced in pharmaceutical factories indicate an annual rise from 100 thousand tons to 200 thousand tons [4–6]. Of grave concern is that these antibiotics are crucial compounds, extensively used to treat many bacterial diseases occurring in both humans and animals. When antibiotics are

carelessly handled or overused, they can, in due course, be found present in the water systems. When these enter the drinking water sources, as well as food crops, they will cause disastrous consequences to public health, and raise the resistance bacteria to antibiotics, now acknowledged as an environmental problem across the world. Besides, when the antibiotics permeate into the soil and ground water, they have detrimental effects on agricultural crops. This affects the plant growth in terms of the ability to impede respiration and impact microbial growth, as well as interfere in the process of nitrification and iron recovery (III). Therefore, there is urgent need to treat and minimize the negative influence exerted by the antibiotics present in the environment [7], particularly in antibiotic-rich wastewater [7–9].

An antibiotic of the Fluoroquinolone class, Ciprofloxacin (CIP: C17H18FN3O3), has broad-spectrum antibacterial action, and is extensively employed in the treatment of aerobic bacterial infections. Therefore, it is very important that effective processes are available to remove the CIP from the aquatic environment and nullify its inherent negative influences [10–12].

Antibiotic-removal from wastewater has been accomplished using a variety of biological treatments like chlorination, filtration, coagulation and sedimentation, phototransformation, ozonation, or processes of advanced oxidation [13–17]. Despite their effectiveness in antibiotic-removal, these methods are not very popular, as they involve high cost, complexity, or release by-products [18, 19].

The adsorption method has been identified as superior to the others cited because of its simple application, effective pollutant removal, and more rapid action; above all, it is easy to use in field conditions and in treatment systems [20–22]. The literature search revealed several works investigating the pharmaceutical-adsorption on activated carbon (AC), clay, carbon nanotubes, silica, and zeolite [23, 24]. The adsorbent with the greatest efficacy is AC, which adsorbs the pharmaceuticals very well, as it has a highly porous and large surface area with the capacity of adsorbing a variety of organic and inorganic elements, even under an extensive range of conditions [25, 26]. Despite the effectiveness of AC and other mesoporous carbon materials as successful adsorbents in CIP-contaminated water, the issue of pollution relentlessly persists because it is hard to actually separate them from the treated wastewater [27, 28]. In reality, the removal of the used adsorbent poses one of the most critical factors from an economical and operational standpoint in the treatment process, particularly in the adsorption method. To find a solution for the separation issue, as well as raise the efficiency of removal through the increase in surface area, one promising method appears to be magnetization of the used adsorbent [29, 30]. Recently, magnetizing the adsorbents using Fe_3O_4 magnetic nanoparticles as a coating was extensively used to heighten the degree of adsorption of the AC and other similar adsorbents, thus enhancing pollutant removal [21, 31, 32].

Although the AC has been identified as the adsorbent with the highest efficiency employed in antibiotic removal, it is not cost-effective on a large scale with regards to synthesis and regeneration. After much research over the last decade, more inexpensive adsorbents have been found to be very effective, which include a variety of non-traditional adsorbents such as rice husk ash, eucalyptus bark, sawdust, Lemna minor (LM), canola, and Azolla filiculoides [33, 34]. In fact, LM, a freshwater plant, the common duckweed, belonging to the genus Lemna, has been identified. As these leaves grow, the plants themselves divide to stand as separate individuals [35, 36]. They grow in freshwater ponds and gently-flowing streams. The LM, also effective as animal feed, is good in nutrient recovery from wastewater, besides its other applications. In the present study, this was the preferred choice, as it could be used a very cost-effective adsorbent [37, 38].

Therefore, the aim of the current study was to synthesize Fe_3O_4-ACLM and investigate its efficiency to adsorb the CIP molecules from aqueous solutions. The characterization parameters relevant to the adsorption process were determined using advanced techniques. Furthermore, the isotherm, kinetic, and thermodynamic processes of CIP adsorption onto Fe_3O_4-ACLM were discussed.

Therefore, the objective of the study presented here was to synthesize Fe_3O_4-ACLM and explore its efficacy in the adsorption of the CIP molecules from aqueous solutions. The characteristic parameters concerned with the adsorption process were identified with the use of advanced techniques. Furthermore, a discussion is presented on the isothermal, kinetic, and thermodynamic processes of CIP adsorption onto the Fe_3O_4-ACLM. Employing five statistical parameters, different isotherms and kinetic models were used to fit the experimental data. Testing was done on the recyclability of the adsorbent in five consecutive adsorption–desorption processes of the CIP.

2 Material and methods

2.1 Chemicals

The Sigma–Aldrich company (Germany) provided the CIP with molecular weight and purity of 385.82 g/mol and 99%, respectively; as well as Acetonitrile of 99.8%, and phosphoric acid of 99.9% purity. Merck (Germany) supplied the other chemicals such as acetic acid (≥ 99.7%), $FeCl_3.6H_2O$

(≥ 98%), $FeCl_2.4H_2O$ (≥ 99%), HCl (36.5%), and NaOH (≥ 98%).

2.2 Preparation and characterization of the Fe_3O_4-ACLM adsorbent

The LM, sourced from the Anzali Wetland, Iran, was used in the preparation of the activated carbon (AC). First, the LM was rinsed using pure water and dried for 1 week, at room temperature. Next, it was subjected to milling and manual sieving through physically shaking the stainless-steel mesh plates having the standard mesh size of 0.45 mm. Therefore, for the AC production, the LM was dried and crushed and 5 g of this was taken (after checking the weight on a digital scale). It was then stirred for 6 h in 40 ml of 28% $ZnCl_2$ solution. Next, it was placed in an electric oven at 105 °C for 24 h and dried. This mixture was then placed in a vertical stainless-steel reactor though which, high purity N_2 gas at 300 cm^3/min flow rate, was passed. The temperature was adjusted to 450 °C and activation was done for 1 h at this temperature.

The excess $ZnCl_2$ was eliminated from the LMAC thus produced, utilizing HCl (0.5 M). The next steps involved filtration and washing with hot water, and final drying (at 105 °C for 24 h). At first, 4 g of LMAC was added to a flask, which was kept for 3 h in an ultrasound bath at 80 °C, to which 20 ml HNO_3 solution (1 M) was poured in. Three hours later, a separation of the LMAC adsorbent from the solution was observed. It was filtered through a filter and dried for 1 day, at room temperature. The Fe_3O_4 nanoparticles and the LMAC, in the ratio of 3:2, were then coagulated in 200 ml distilled water. This was transferred to an ultrasound bath for 1 h maintaining the temperature at 80 °C. The Fe_3O_4-ACLM thus prepared was then filtered and thrice washed with distilled water and rinsed well once with ethanol (200 ml). Finally, the Fe_3O_4-ACLM was oven-dried for 24 h at 100 °C.

The excess $ZnCl_2$ was removed from the LMAC produced, with the aid of HCl (0.5 M). Next, the LMAC was filtered and washed using hot water and ultimately dried for 24 h (at 105 °C). Now, 4 g of the LMAC was put in a flask and kept in an ultrasound bath for 3 h at 80 °C, to which 20 ml of HNO_3 solution (1 M) was added. Three hours later, separation of the LMAC adsorbent from the solution was done through filtration, and dried for 1 day at room temperature. Next, coagulation of the LMAC was done using the Fe_3O_4 nanoparticles in a 2:3 ratio in 200 ml of distilled water. This was then kept in an ultrasound bath for 1 h at 80 °C. The Fe_3O_4-ACLM thus prepared was filtered and thrice washed using distilled water and rinsed once using 200 ml of ethanol. Finally, the Fe_3O_4-ACLM was oven-dried for 24 h maintaining the temperature at 100 °C.

The TEM model (LEO 912 AB) was used in this study, at 100 kV, and the SEM/EDX (MIRA3 FEG-SEM-Tescan) was also employed to ascertain the size, shape, and morphology of the Fe_3O_4-ACLM. Then, using the KBr pellet method, the FTIR (Thermo Nicollet AVATAR5700) was also employed, keeping the range between 4000 and 400 cm^{-1}. Using the nitrogen adsorption at – 196 °C in a Micromeritic Model ASAP 2020 Plus, the specific surface area and pore size values were evaluated through the Brunauer–Emmett–Teller (BET) and Barrett–Joyner–Halenda (BJH) analyses. Further, with the help of a vibrating sample magnetometer (VSM) (Micromeritics Instrument Corp., Norcross, GA, USA), the magnetization curves were identified at 300 K, in a 50 KOe applied field.

2.3 Batch adsorption tests

The batch mode was used for the CIP adsorption studies. The adsorption experiments were conducted using 250 ml Erlenmeyer flasks containing different concentrations (25–100 mg/L) of the CIP ionic solution. First, 0.5 g of pure CIP powder was dissolved in 1 L of distilled water to produce 500 mg/L of CIP stock solution. The stock solution was diluted to prepare the test concentrations required. Next, the necessary quantity of Fe_3O_4-ACLM was added to the solution. The flasks were placed on an electrical thermostatic shaker at 120 rpm and stirred. The effect exerted by the various experimental parameters for CIP removal were examined, keeping the pH in the 3–11 range. The parameters included the dose of Fe_3O_4-ACLM (0.1 to 1 g/L), initial CIP concentration (25–100 mg/L), contact time (10–150 min), and temperature (20–50 °C).

The experiments were performed adopting the optimization method, so that when only one parameter was changed, while keeping the others constant, the optimal value of the variable parameter was easily calculated. In this study, both the initial concentration and contact time were optimized and tested using different concentrations, from 25 to 100 mg/L, as well as different contact times (10–150 min), but taking care to maintain the adsorbent dose, pH, and temperature at constant. Once the optimal concentration and contact time were obtained, the other parameters were examined at that optimal concentration and contact time.

After the Fe_3O_4-ACLM was separated using a strong magnet, the supernatant was drawn off with the help of a 0.22 µm polypropylene membrane syringe filter. All the tests were done twice, using the mean data to record the results. The CIP in all the samples was ascertained using the column HPLC (C18 ODS) and a 2006 UV detector at 277 nm. The mobile phase included 0.05 M phosphoric acid/acetonitrile with 87/13 volume ratio and 1 ml/min flow rate of the injection. The solution pH was considered adjusted by using either 0.1 M HCl or 0.1 M NaOH.

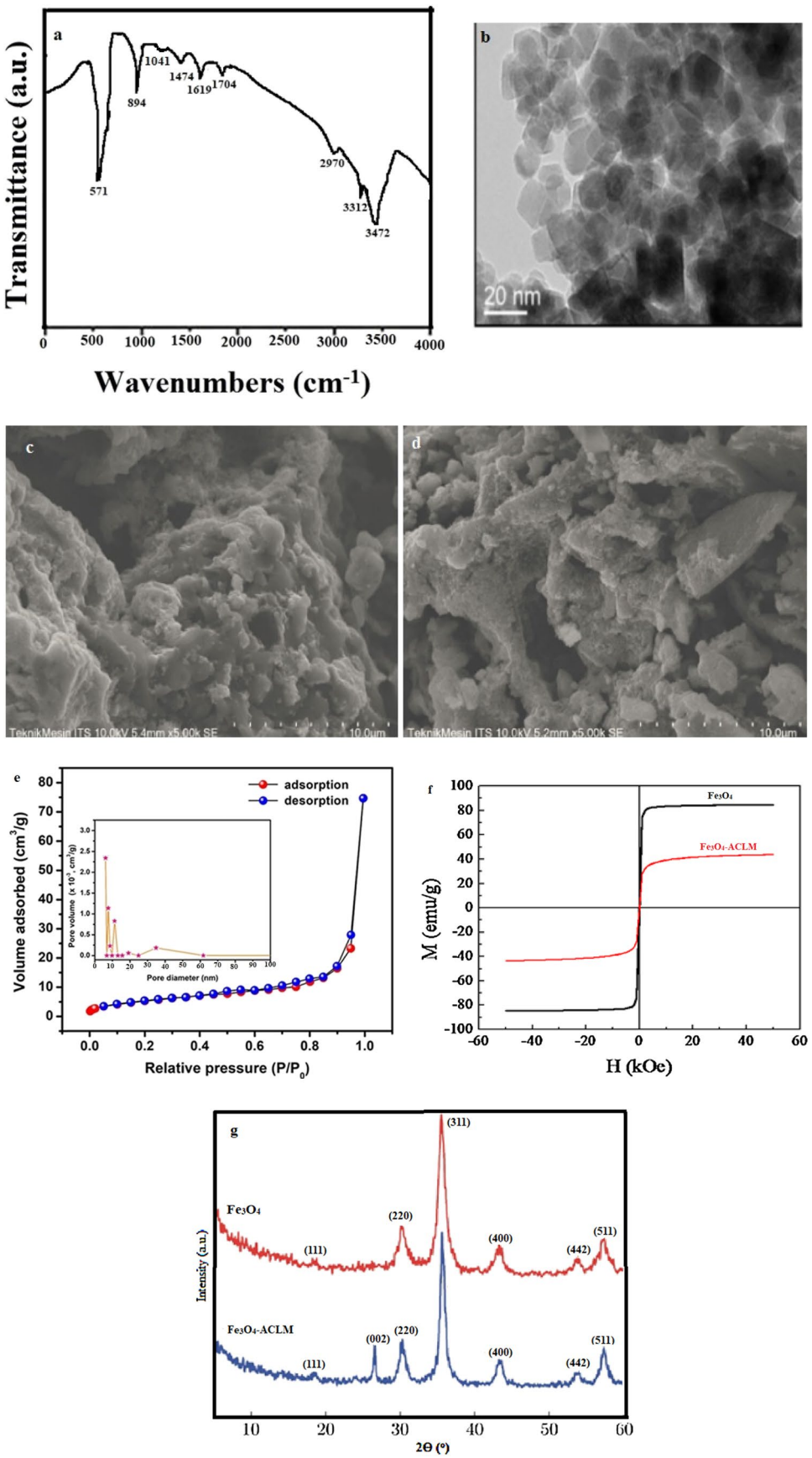

Fig. 1 The FTIR (**a**), TEM (**b**), SEM (**c**, **d**), BET (**e**), the magnetic hysteresis loops (**f**), and XRD (**g**) analysis

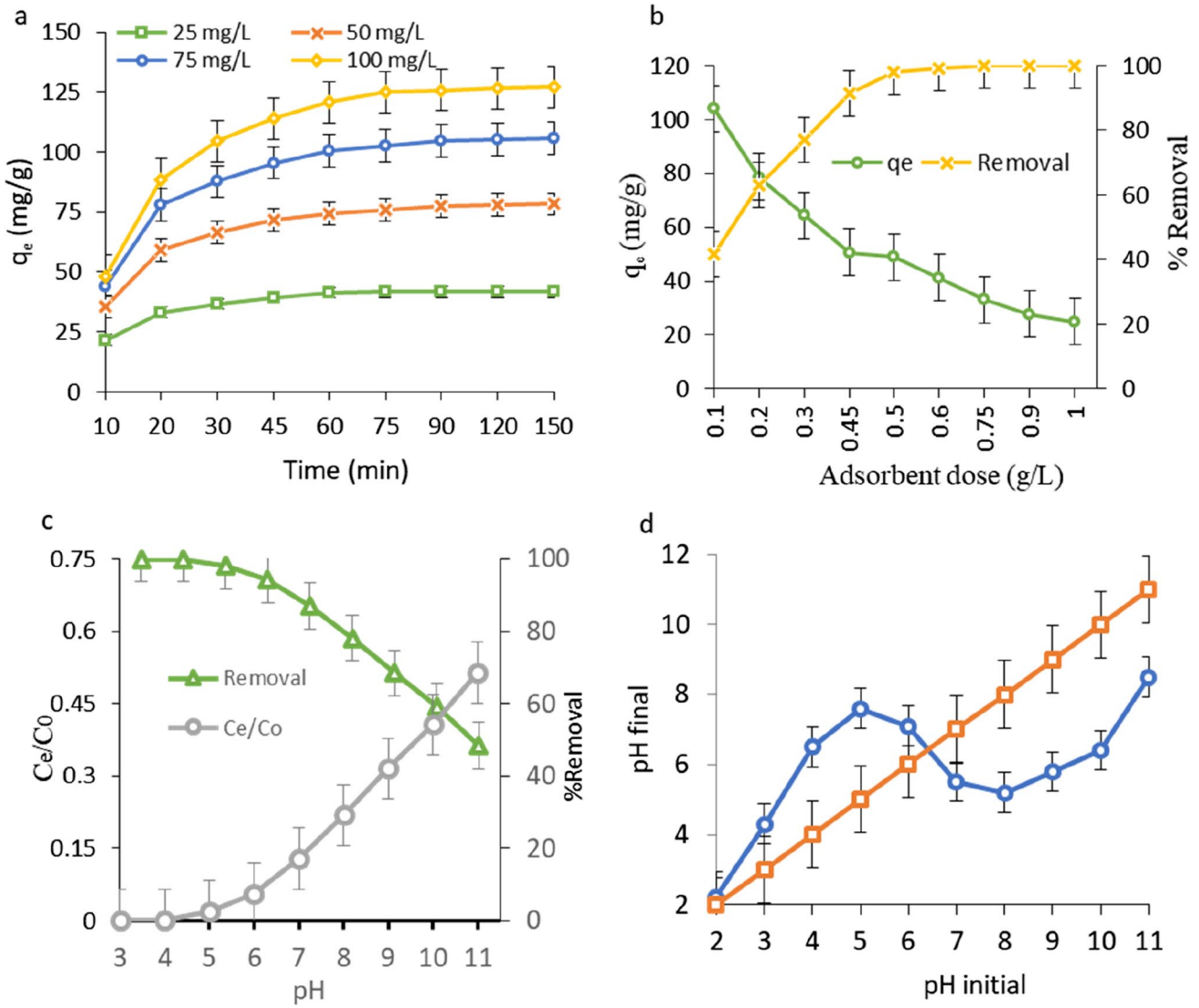

Fig. 2 The effect of the initial CIP concentration (**a**), adsorbent dose (**b**), pH (**c**), and pH_{pzc} analysis (**d**)

Calculation of the adsorption capacity (q_e) and removal efficiency (% Removal) using general Eqs. 1 and 2 [39]:

$$q_e = \left(\frac{C_0 - C_e}{\mathrm{M}}\right) \times \mathrm{v} \tag{1}$$

$$\%\mathrm{Removal} = \left(\frac{C_0 - C_e}{C_0}\right) \times 100 \tag{2}$$

where q_e refers to the mg of the absorbed CIP on 1 g of Fe_3O_4-ACLM; V (L) indicates the volume of the solution which contains the CIP, in contact with the Fe_3O_4-ACLM; *Co* and *Ce* imply the initial concentration and equilibrium (residual) of CIP in the solution (mg/L), respectively; and M (g) is the quantity of the added Fe_3O_4-ACLMinto the solution.

2.4 Error analysis

The model most compatible with the experimental data was determined by ascertaining and comparing the correlation coefficients (R^2). Thus, to identify the most suitable model, the R^2 value is the best criterion; however, there are limitations in solving the nonlinear isotherm models because they require the utilization of different parameters. Hence, in this study, in order to determine the most appropriate model, five different error functions were employed. The error functions, used in this study, therefore are expressed in the equations given [40–42].

$$\mathrm{SSE} = \sum_{i=1}^{n} (q_{ecal} - q_{emeas})_i^2 \quad \mathrm{Sumofsquarederrors} \tag{3}$$

$$\mathrm{SAE} = \sum_{i=1}^{n}(q_{ecal} - q_{emeas})_i \quad \text{Sum of absolute errors} \tag{4}$$

$$\mathrm{ARE} = \frac{100}{n}\sum_{i=1}^{n}\left(\frac{q_{ecal} - q_{emeas}}{q_{emeas}}\right)_i \quad \text{Average relative error} \tag{5}$$

$$\mathrm{HYBRID} = \frac{100}{n-p}\sum_{i=1}^{n}\left[\frac{(q_{emeas} - q_{ecal})_i^2}{q_{emeas}}\right] \quad \text{Hybrid fractional error function} \tag{6}$$

$$\mathrm{MPSD} = 100\sqrt{\frac{1}{n-p}\sum_{i=1}^{n}\left(\frac{q_{e\,meas} - q_{e\,cal}}{q_{e\,meas}}\right)_i^2} \quad \text{Marquarts percentage standard deviation} \tag{7}$$

where q_{emeas} and q_{ecal} are the experimental and calculated uptakes, respectively.

3 Results and discussion

3.1 FTIR analysis

FTIR was one of the analyses performed for the adsorbent synthesized in this study, i.e., the Fe_3O_4-ACLM, performed in the 4000–400 cm^{-1} range (Fig. 1a). The dried sample was first placed on a silicon substrate, transparent to the infrared, and the spectra were measured according to the transmittance method [43]. From the FTIR spectrum, evidence of a very strong band was visible at 3312 cm^{-1}; this is attributed to the O–H stretching of the hydrogen-bonded hydroxyl groups. The absorption peak at 3472 cm^{-1} may be caused due to the N–H stretching which implies the presence of free and intermolecular-bonded hydroxyl groups resulting from the alcoholic or phenolic functions and amine group. The findings of this analysis indicate the likelihood of an absorption band at 1704 cm^{-1}; this suggests the stretching vibration caused by the carboxyl group (C = O), related to the acid molecule, which becomes adsorbed onto the surfaces of the composites. At 1619 cm^{-1}, the peak noticed was found to be linked to the carboxylate (COO-) stretching vibration which could be due to the lignin aromatic group; a band present at around 1474 cm^{-1} is supposed to be due to the $–CH_2$ deformation bending. The strong -C-O band visible at 1041 cm^{-1} resulting from the $–OCH_3$ group is because of the lignin structure present in the LM head, the characteristic peak of the polysaccharides [32]. The peaks observed at 894 cm^{-1} and 571 cm^{-1} may be caused due to the vibrations of the Fe–O bond for FeO(OH), as well as the Fe–O bond, respectively, which lends support to the Fe_3O_4-ACLM nanoparticles present there.

3.2 TEM images

The TEM images of Fe_3O_4-ACLM are shown in Fig. 1b. The TEM images of the Fe_3O_4-ACLM (1b) thus prepared indicate the very porous structure of adsorbent, with an abundance of both micropores and mesopores. Further, the Fe_3O_4 NPs are extensively dispersed on the ACLM surface and reveal an almost spherical morphology, with diameter of almost uniform size of 9.8 ± 1.5 nm, in fact concurring with the BJH analysis.

3.3 SEM images

The SEM images shown in Fig. 1c, d reveal the morphology and microstructure of the Fe_3O_4-ACLM prior to and post the adsorption process; according to this, several pores and holes are present on the external Fe_3O_4-ACLM surface, suggesting the existence of a variety of sizes and shapes for the magnetite Fe_3O_4-ACLM. Further, prior to the CIP adsorption, the Fe_3O_4-ACLM appeared to have irregular shape and a rough surface, as shown in Fig. 1c. However, post the adsorption, the Fe_3O_4-ACLM showed a flatter surface morphology, as shown in Fig. 1d, caused by the CIP covering the Fe_3O_4-ACLM adsorbent surface. Besides, a few white particles evident on these sample surfaces were most likely iron oxide nanoparticles, implying the creation of a layer of neatly dispersed iron particles on the surface of the adsorbent. Identical features were also reported by Balarak on the activated carbon surface derived from Azolla filiculoides [34].

3.4 BET analysis

From the BET analysis, it was evident that at 582 m^2/g the specific surface area of the Fe_3O_4-ACLM was a little smaller than that of the ACLM (645 m^2/g). The reason for this condition is due to the Fe_3O_4 covering the AC surface; in fact, this resulted in the slightly lower specific surface area of the Fe_3O_4-ACLM adsorbent. The BET analysis (Fig. 1e) was done to investigate the microstructure of the Fe_3O_4-ACLM. According to the IUPAC classification, a typical type IV isotherm was obtained for the Fe_3O_4-ACLM, which is characteristic for porous materials. From the study of the BJH pore size distribution, the

Table 1 Characteristic of the Fe_3O_4-ACLM and ACLM

Adsorbent	C%	Moisture %	Pore volume (cm^3/g)	Average pore diameter (nm)	H%	Fe%	N%	O%
Fe_3O_4-ACLM	45.1	1.6	0.695	9.5	3.7	7.9	0.95	42.2
ACLM	50.8	1.2	0.604	7.4	4.6	–	1.04	43.4

recovered Fe_3O_4-ACLM showed the presence of pores, having diameters in the 8 to 12 nm range.

A summary of the results regarding the properties of the Fe_3O_4-ACLM and ACLM are shown in Table 1, which include moisture content, total pore volume, and a number of various elements, etc.

The magnetic hysteresis loops of the Fe_3O_4-ACLM and Fe_3O_4 are revealed in Fig. 1f. From these results, it was clear that the value of the magnetization saturation (Ms) for the Fe_3O_4-ACLM nanoparticles was 37.6 emu/g, whereas for the Fe_3O_4 nanoparticles it was 81.2 emu/g. The characteristic superparamagnetic behavior was detected for both materials, recognized by the typically shaped curve [38]. On comparing the results found for the Fe_3O_4-ACLM and Fe_3O_4, a reduction in the magnetic response for Fe_3O_4-ACLM was noted, most likely due to the layers of magnetic material present in the carbon structure. Hence, the Fe_3O_4-ACLM and Fe_3O_4 (having high Ms values) can reveal a quick response to the external magnetic field, which in turn will cause these adsorbents to rapidly separate from the aqueous CIP solution.

3.5 XRD analysis

The X-ray powder diffractograms of the Fe_3O_4-ACLM and Fe_3O_4 nanoparticles are seen in Fig. 1g. These patterns reveal a series of typical peaks (220), (311), (400), (111), (511), and (442), which concur well with the inverse cubic spinel phase of the Fe_3O_4 (magnetite, JCPDS card no. 85–1436). Using Scherrer's formula, the mean diameter of the crystallite deduced from the diffractogram by [40] is 11 nm. This confirms the size perceived by the BJH distribution of pore size. Additionally, from the XRD pattern, the characteristic peaks of carbon, of about 27°, were observed at 2θ; this supports the fact that amorphous carbon is present. From the intensity of the peaks and their rather narrow widths, a high level of crystallinity is indicated in the nanocomposite [39].

3.6 Effect of different parameters on CIP adsorption

The influence exerted by the initial CIP concentration and contact time are evident in Fig. 2a. As cited, any increase in the concentration of the initial CIP is related to an improvement in the capacity of the CIP to be adsorbed onto the Fe_3O_4-ACLM. At the initial contact time, rapid adsorption was noted, connected to the abundance of the available active sites on the surface of the adsorbent material [40]. As these active sites were gradually occupied, efficient adsorption was observed to decrease. Further, the increase in the initial CIP concentration is linked to the rise in the quantity of the CIP adsorbed; this occurs because of the availability of the higher gradient of available molecules in the medium, which caused a rise in diffusion during the process of mass transfer [41]. Although the data collection was done at the contact time of 150 min, the equilibrium time of the adsorption process took only 75 min. The findings from this study concurred with those reported in earlier studies [44, 45].

In Fig. 2b, it is evident that the removal percentage (%) and adsorption capacity (q_e) of CIP is given against the dose of the Fe_3O_4-ACLM. The results implied an increase in the removal percentage in response to an increase in the Fe_3O_4-ACLM dose; this occurs due to the greater number of active sites available for adsorption. However, when the quantity of the Fe_3O_4-ACLM is increased, the adsorption capacity (q_e) is observed to decrease; a reduced quantity of the CIP adsorbed per gram of Fe_3O_4-ACLM could be regarded as the cause for this occurrence. Another plausible reason could be the adsorption sites overlapping or aggregating, which ultimately resulted in reducing the total specific surface area of the Fe_3O_4-ACLM available and promoting the route for diffusion [41].

The influence exerted by pH on the CIP adsorption by Fe_3O_4-ACLM, as well as its optimum, was determined to be in the 3.0–11.0 range, and the results are shown in Fig. 2c. In the course of conducting this part of the experiments, the constant values of the initial concentration of the CIP (25 mg/L), Fe_3O_4-ACLM dose (0.6 g/L), temperature (30 ± 2 °C), and contact time (75 min) were taken into account. The adsorbent in this study revealed a pH_{pzc} value of 6.4 (Fig. 2d). From these results, it was evident that the Fe_3O_4-ACLMto anionic molecules tended to be greater when the pH value dropped below the pH_{pzc}, a phenomenon understood as an increase in the cations on the carbon surface. In fact, when the pH values exceed that of the pH_{pzc}, there is heightened adsorption of the cationic compounds [30]. When the CIP gets disassociated in water, the anionic molecules are formed; it is, therefore, anticipated that, at pH values less than the pH_{pzc}, the Fe_3O_4-ACLM acts as a potential CIP adsorbent. On comparison of the removal efficiencies at different pH values, the CIP adsorbed starts to reduce as the pH rises. For the amine and carboxylic acid groups in the piperazine moiety, the pKa values for the CIP are 8.7 and 6.1, respectively. When the pH of the solution drops below 6.1, the CIP is observed most often as a cation; however, when the pH hovers in the range of 6.1 to 8.7, the CIP is zwitterionic. When the pH of the solution exceeds 8.7, the CIP loses the protons of the carboxylic group, and appears mostly as anions. When the pH plummets to less than 6.1, there is a rise in the CIP removal because the electrostatic attraction increases due to the opposite charges between the CIP and Fe_3O_4-ACLM. Earlier studies done on the CIP adsorption employing different adsorbents reported similar findings [7, 9].

3.7 Isotherm studies

The adsorption equilibrium isotherm is usually used to explain the adsorption properties. In the present study, the Langmuir, Freundlich, Temkin, and D-R isotherms were used to investigate the equilibrium adsorption of the CIP by Fe_3O_4-ACLM (Table 2). To gain greater knowledge regarding the theoretical background of the isotherm model, the following references have been referred [25, 46]. As evident from Table 2, the maximum adsorption is achieved with the rise in temperature, with better performances revealed at the high temperatures, also concurrent with the thermodynamic adsorption findings. From these isotherm studies, the R^2 values obtained for a model under investigation for the present adsorption system is in the order as given: Langmuir > D-R > Temkin > Freundlich. According to the order mentioned, for the present study, the higher R^2 values (0.995–0.998) were linked to the Langmuir isotherm model, suggesting the incidence of the monolayer coverage of the pollutant molecules on the surface of the Fe_3O_4-ACLM. At different temperatures, the q_m values obtained for the Langmuir isotherm equation were 134.2, 149.5, 161.4, and 178.7 mg/g, respectively.

For the Temkin model, the values of B were found to be below 1 signifying that the adsorption process of the CIP onto the Fe_3O_4-ACLM is endothermic in nature, at the concentration under investigation. Finally, based on the mean adsorption energy (E) drawn from the D-R isotherm model, it was evident that there was a significant part for the hydrophobic effect, hydrogen bonding, electrostatic attractions, and interaction between Fe_3O_4-ACLM and CIP to play, in this adsorption process.

Also, for the D-R isotherm, parameter E dropped below 8 kJ/mol at the low temperatures and exceeded 8 kJ/mol at the high temperatures, suggesting that at low temperatures the CIP adsorption is a physical process, while at the higher temperatures the chemical reactions are the ones assisting in the adsorption process [35]. Also, for the Langmuir isotherm at each temperature, the R_L parameter was found to hover between zero and one, indicating that the uptake of the CIP by the Fe_3O_4-ACLM was optimal [47].

In Table 2, the results of the error analyses for the different isotherms are shown and as is evident, the Langmuir isotherm, at all temperatures, reveals a higher regression coefficient and a lower error coefficient. In Table 3, a comparison is made of the maximum adsorption capacity as calculated from the Langmuir isotherm for the CIP adsorption

Table 2 Isotherm parameters for adsorption of CIP on Fe_3O_4-ACLM at various temperatures

Models	293 K	303 K	313 K	323 K	Models	293 K	303 K	313 K	323 K
Langmuir	$\frac{Ce}{qe}=\frac{1}{q_m K_L}+\frac{Ce}{q_m}$, $R_L=\frac{1}{1+K_L C_0}$ K_L = Langmuir isothermal constant (L/mg) and R_L = separation factor				Temkin	$q_e=\frac{RT}{b} ln\, A+\frac{RT}{b} Ln\, C_e$, $B=\frac{RT}{b}$ A = equilibrium binding constant (L/mg), b = maximum theoretical heat of adsorption (J/mol)			
q_m	134.2	149.5	161.4	178.7	A	21.2	34.1	38.7	46.4
K_L	0.0024	0.0027	0.0035	0.0044	b	0.721	0.795	0.871	0.825
R_L	0.806	0.787	0.741	0.694	R^2	0.876	0.882	0.891	0.873
R^2	0.997	0.997	0.995	0.998	SSE	11.1	8.41	11.2	9.56
SSE	1.45	2.17	1.44	1.46	SAE	9.21	9.25	9.43	8.14
SAE	1.89	1.63	1.89	2.45	HYBRID	8.25	6.4	10.3	10.5
HYBRID	2.27	1.07	1.37	2.68		7.35	7.93	7.24	7.41
ARE	1.73	3.06	2.45	3.12	ARE	6.38	8.52	9.14	6.64
MPSD	2.56	1.25	2.53	1.23	MPSD				
Freundlich	$log\, q_e=\frac{1}{n} log\, Ce+log\, K_F$ K_F = (mg/g (mg/L)$^{1/n}$) and n are constants that depend on temperature and are related to the adsorption capacity and intensity				D-R	$lnq_e=lnq_m—B\varepsilon^2$ $E=\frac{1}{2B^{0.5}}$ B = a constant related to the sorption energy (mol^2/J^2), ε = Polanyi potential (kJ/mol), E = adsorption energy (J/mol)			
K_F	2.49	4.06	5.32	5.63	q_m	78.6	94.3	102.1	109.5
1/n	0.425	0.476	0.573	0.643	E	4.17	6.79	8.14	8.93
R^2	0.876	0.901	0.823	0.867	R^2	0.952	0.964	0.973	0.958
SSE	3.54	7.14	10.34	11.35	SSE	11.7	13.4	8.41	11.3
SAE	4.59	6.78	8.98	9.72	SAE	9.24	11.2	14.2	13.2
HYBRID	5.65	9.14	7.43	8.31	HYBRID	10.6	9.23	9.26	15.3
ARE	7.14	8.42	8.41	9.25	ARE	7.25	10.7	10.6	8.41
MPSD	4.56	7.56	9.15	6.14	MPSD	5.39	11.5	11.8	9.42

with a similar research study done on the elimination of this antibiotic; of note, a large percentage of these studies have been conducted over the recent years, and the findings reveal Fe_3O_4-ACLM to have the highest efficiency when compared to other similar adsorbents, as displayed in Table 3.

3.8 Adsorption kinetics

From Fig. 3a, it is evident that the initial adsorption rate was so high that 80% of the adsorption occurred at 25 mg/L concentration within the first 30 min of the process; this was caused by the high concentration gradient and the absence of adsorption by the adsorbent at the commencement of the process [44]. Moderate processing speed was seen from 30 to 60 min, which escalated in a gentle gradient, and no adsorption was noted from 60 min onwards, the reason for the reduction at the adsorption sites.

Using adsorption kinetics, the reaction rate and paths can be understood, and are dependent upon the physical and chemical characteristics of the adsorbent. Three models were employed to explain the adsorption kinetics, namely the pseudo-first-order kinetics (PFO), pseudo-second-order kinetics (PSO), and intra-particle diffusion (IPD) models [55, 56].

In fact, Table 4 reveals the equations for the kinetics, in addition to the analysis of the results. As shown in Table 4 and Fig. 3b, c, the equilibrium data at all the concentrations investigated appear to satisfy the PSO model more than the PFO kinetic model. Further, the error coefficients for the PSO model were lower than those of the PFO kinetic one, and finally, the results recorded from calculating the experimental q_e and q_e drawn from the PSO model show closeness to each other, revealing smaller number of differences and greater consistency. Notably, the results of the q_e exp for the concentrations of 25, 50, 75, and 100 mg/L were found equal to 41.6, 78.25, 105.6, and 127.1 mg/g, respectively; however, a comparison of these numbers with q_e assessed from the PFO model, as given in Table 2, is very different. Therefore, it is evident that in all respects the equilibrium data follow the PSO kinetics.

The IPD was used to study the adsorption mechanism and the equation is given in Table 4. The degree of effectiveness of the boundary layer thickness is determined from the value of C in the IPD equation. From this, it appears the higher C values indicate the important impact exerted by the boundary layer. When the adsorption process is under the direction of the IPD, plotting the q_t versus $t^{1/2}$ (Fig. 4d) results in a linear plot.

The IPD is introduced as a rate-controlling step only if the lines obtained cut through the origin. Else, other factors, like the boundary layer diffusion (or external mass transfer), barring the IPD, exert influence on the adsorption process. From Fig. 3d, it is evident that there are three different phases of the process, namely surface sorption, intra-particle diffusion, and a likely chemical reaction step. The last of the stages cited above is insignificant and occurs rapidly. Table 4 lists data including the k and C values for all the three stages, obtained by fitting the data acquired to the IPD model. A critical factor that has been introduced is the driving force for the adsorption processes. The boundary layer diffusion also is crucial to the adsorption process as the regression of q_t versus $t^{1/2}$ has not cut through the origin. The higher C values acquired for all the kinetic studies indicate the role of the IPD in the process of adsorption. However, barring the IDP, there are other factors which also control the process under investigation [57, 58].

Table 3 Comparison of the maximum adsorption values of various adsorbents for CIP

Adsorbent	q_m (mg/g)	Reference
Kaolinitic clay	21.76	[47]
SBA-15	29.14	[48]
Granular AC	38.49	[20]
Carbon xerogel	45.2	[10]
AC-palm leaflets	48.91	[12]
Schorl	56.95	[49]
Bamboo charcoal	59.35	[50]
Birnessite	66.79	[51]
AC- Jerivá	65.9	[13]
MACC	71.11	[14]
MgO nanoparticles	84.93	[52]
CuO nanoparticles	89.46	[53]
Microwave pyrolysis	93.16	[54]
$ZnO/BaTiO_3$	125.29	[23]
Fe_3O_4-ACLM	178.7	This study

3.9 Effect of temperature and determination of thermodynamic parameters

From the findings arrived at in this study, the highest removal percentage was observed at 323 K, indicating that the adsorption process was endothermic (Fig. 4a). When the ions increased in mobility in response to a rise in the temperature, the interaction between the ions and the Fe_3O_4-ACLM surface was enhanced, which may be the likely cause for the results in this section [59].

Through the use of thermodynamic studies, the physical or chemical nature of the adsorption mechanism is understood. In order to calculate the elimination of CIP by Fe_3O_4-ACLM, the thermodynamic parameters, namely standard Gibb's free energy (ΔG^0), standard enthalpy (ΔH^0), and standard entropy (ΔS^0), were used, as shown in the equations given here [60].

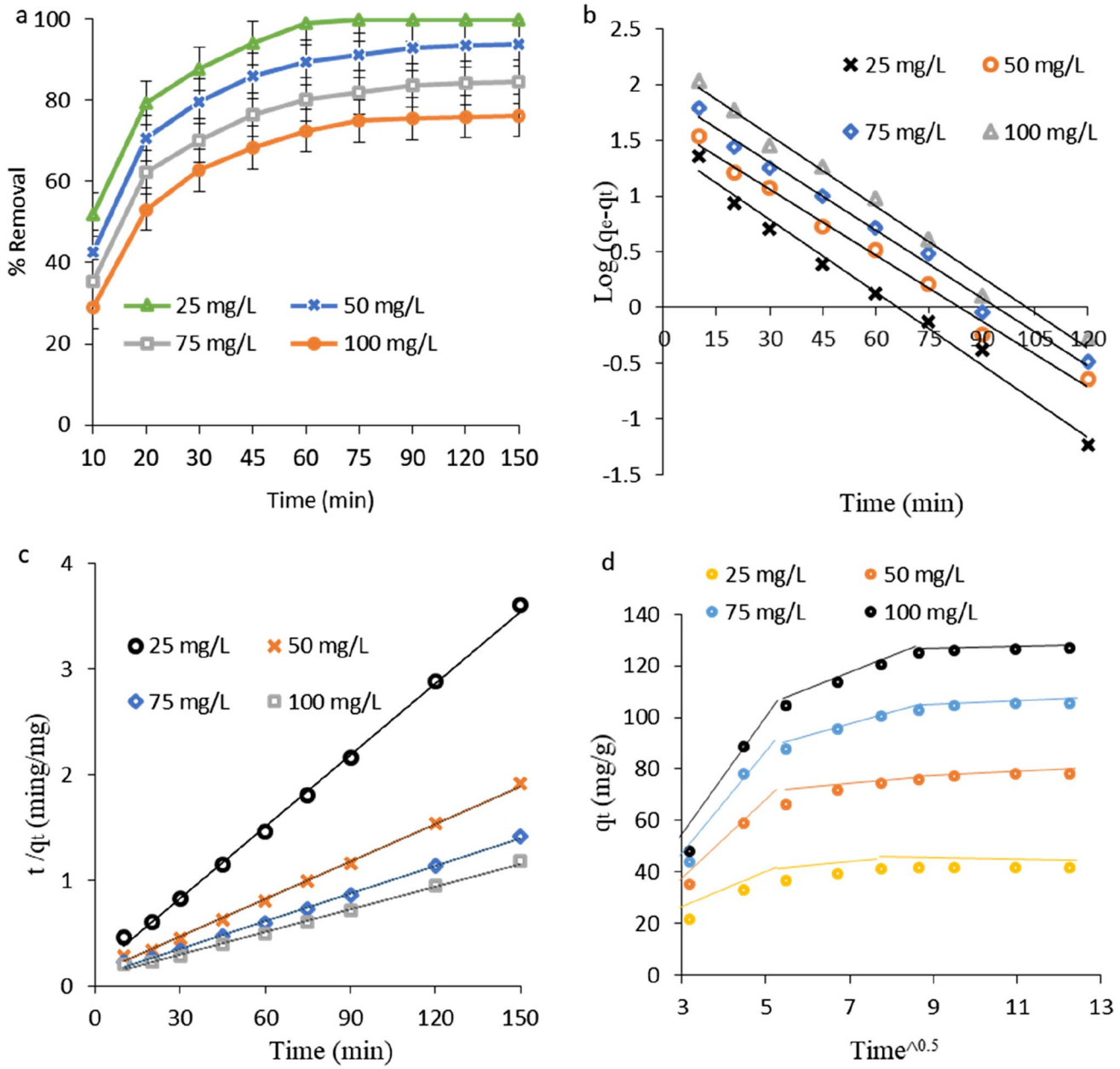

Fig. 3 The effect of the initial CIP concentration on the removal % **a** pseudo-first-order kinetic model, **b** pseudo-second-order kinetic model, **c** intraparticle diffusion model, and **d** of the CIP adsorption on Fe_3O_4-ACLM

$$\Delta G^0 = -RTLnK \tag{8}$$

$$LnK = \left(\Delta S^0/R\right) - \left(\Delta H^0/RT\right) \tag{9}$$

where R (8.314 J/mol K) is the universal gas constant; K refers to the constant drawn from the Langmuir equation, and T implies the absolute temperature (K). The thermodynamic parameters for the CIP adsorption onto the Fe_3O_4-ACLM surface at various temperatures are noted in Table 5.

The possibility of the adsorption process and its spontaneous nature are indicated by the negative value of ΔG^0 in Table 5. This concurs with the results attained from the Langmuir R_L separation factor, where the R_L values hover from 0 to 1 ($0 < R_L < 1$) and the Freundlichn symbol exceeds 1. Notably as the temperature increased, the value of ΔG^0 reduced, implying that the adsorption process is enhanced by a rise in temperature [61]. When the ΔH^0 value is positive, it indicates the endothermic and irreversible nature of the adsorption process [62]. Further, the positive values of ΔS^0

Table 4 Kinetic parameters for the CIP adsorption on Fe_3O_4-ACLM

Model	Parameters	25 mg/L	50 mg/L	75 mg/L	100 mg/L
PFO $Log\ (q_e - q_t) = log\ q_e - \frac{K_1}{2.303}\ t$ q_e = adsorption capacity at equilibrium time and q_t = adsorption capacity at time t (mg/g), K_1 (1/min) = equilibrium rate constant for PFO	$q_{e\ (cal)}$	28.4	35.7	51.9	72.8
	K_1	0.049	0.045	0.046	0.048
	R^2	0.986	0.991	0.982	0.987
	SSE	8.95	11.2	14.48	8.46
	SAE	10.1	13.4	8.34	7.56
	HYBRID	7.44	7.83	8.92	6.45
	ARE	6.57	9.26	7.27	9.78
	MPSD	11.2	8.59	11.4	7.23
PSO $\frac{t}{q_t} = \frac{1}{K_2 q_e^2} + \frac{t}{q_e}$ K_2 (g/mg. min) = equilibrium rate constant for PSO	$q_{e\ (cal)}$	44.15	84.03	114.9	140.84
	K_2	0.0034	0.0012	0.0008	0.0005
	R^2	0.998	0.998	0.997	0.995
	SSE	1.25	1.44	1.95	2.11
	SAE	3.76	2.23	2.49	2.87
	HYBRID	1.12	1.89	2.79	3.44
	ARE	1.19	2.57	1.84	1.27
	MPSD	1.76	2.36	3.58	1.06
IPD $q_t = K_b\ t^{1/2} + C$ K_b = IPD rate constant (mg/g. $min^{1/2}$) C = boundary layer thickness	Stage 1				
	K_b	6.55	13.6	19.2	24.6
	C	1.75	5.98	14.1	27.2
	R^2	0.951	0.955	0.946	0.972
	Stage 2				
	K_b	1.22	2.21	3.64	4.78
	C	31.24	56.9	71.39	98.9
	R^2	0.885	0.977	0.969	0.995
	Stage 3				
	K_b	0.01	0.292	0.332	O.459
	C	41.53	74.7	101.6	121.4
	R^2	0.958	0.956	0.983	0.997

also suggest the affinity of the Fe_3O_4-ACLM surface for the CIP ions and the high degrees of disorder and randomness at the solid-solution interface [63].

3.10 Ionic strength test

From prior investigations, ion strength apparently affects the electrostatic interactions between the adsorbents and pollutants. In the meanwhile, electrolytes also influence the adsorption process as they compete with the pollutant ions for adsorption onto the surface of the adsorbent [58]. The effect exerted by this parameter on the CIP adsorption onto the Fe_3O_4-ACLM is evaluated, as shown in Fig. 4b which suggests that ionic strength has a negative relationship with the capacity for CIP adsorption.

The reason for this, most likely, is that when the pH is acidic, any increase in the concentration of the other ions raises the competition for adsorption onto the adsorbent surface, while simultaneously neutralizing the positive charge carried by the adsorbent surface; in addition, there is a rise in the electrostatic repulsion between CIP molecules to be adsorbed and the surface of the Fe_3O_4-ACLM adsorbent [59].

3.11 Reusability of Fe_3O_4-ACLM

Recovery and reusability are the critical parameters assessed for the selection of an adsorbent which is cost-effective and practical for use in pilot-scale treatment systems. The reusability of the adsorbent synthesized in the present study was considered, i.e., Fe_3O_4-ACLM was assessed by performing CIP adsorption cycles (CIP = 25 mg/L). From Fig. 4c, the results drawn from the experiments done to evaluate the recyclability and stability of the Fe_3O_4-ACLM adsorbent can be seen; all the experiments were performed within 75 min of contact time. Recycling and reuse of the adsorbent synthesized in this work can be performed easily using a strong magnet, post treatment. In our findings, a drop from ~ 100 to ~ 91% (by only 9%) in the adsorption activity of Fe_3O_4-ACLM was identified after six successive cycles.

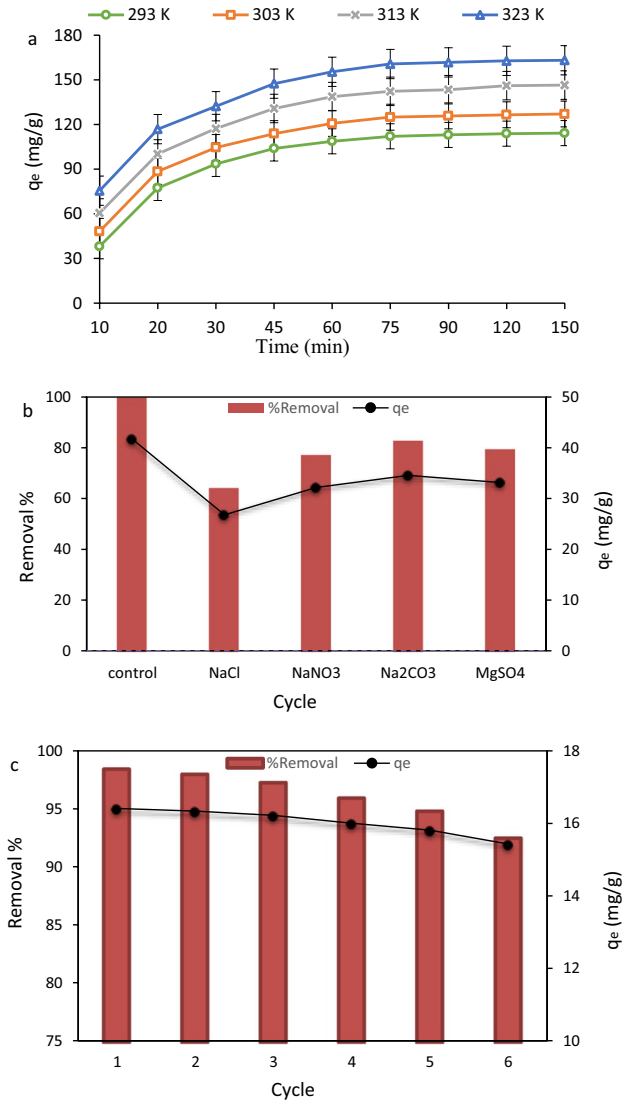

Fig. 4 Effect of temperature on q_e (**a**), ionic strength effect on CIP adsorption on Fe_3O_4-ACLM (**b**), and Fe_3O_4-ACLM recyclability experiment (**c**)

Table 5 Values of thermodynamic parameters for the adsorption of CIP on Fe_3O_4-ACLM

Temperature (K)	ΔG^0 (kJ/mol)	ΔH^0 (kJ/mol)	ΔS^0 (kJ/mol K)
293	−2.99	65.07	0.201
303	−4.03		
313	−5.91		
323	−10.17		

Two reasons have been put forward for this marginal reduction in the adsorption activity. In the recovery phase, when washing and drying are done, material losses may take place, resulting in a decrease in the adsorbent dose in the next cycle, which causes the surface adsorbent activity to decline, thus lowering the efficiency. Further, the likely alterations in aggregation and fouling properties of the magnetic nanoparticles in those six cycles can be understood as the other reason for the event cited above. Based on the documents available, aggregation can cause the effective surface area to decrease and the number of active sites to reduce.

4 Conclusion

The present study included the preparation of activated carbon from the Lemna minor plant which was magnetized using Fe_3O_4 nanoparticles, done using both chemical and physical techniques. The adsorbent thus prepared was investigated for its efficacy in the elimination of the antibiotic ciprofloxacin (CIP) from aqueous solutions. Here, $ZnCl_2$ was used as the dehydration agent in the chemical activation process; the high temperature heating process was employed for the physical activation. The maximum CIP removal efficiency (100%) was achieved under the following conditions: initial CIP concentration = 25 mg/L, solution pH = 3, Fe_3O_4-ACLM dose = 0.75 g/L, and adsorption time = 75 min. From the kinetic results, the involvement of more than one mechanism was evident in the adsorption process, with the possibility of intra-particle diffusion and film diffusion control also playing a role in the adsorption process. Besides, it was found that the pseudo-second order models showed higher suitability to describe the kinetics data, a fact confirmed by the findings of the parameters of goodness-of-fit. From the experiments of sequential adsorption and desorption, it was clear that the successful reusability of the Fe_3O_4-ACLM was possible for six cycles, with the adsorption efficiency revealing only 9% reduction. From the linear regression with five error functions showed it was clear that the Langmuir model could be used to describe the CIP adsorption on Fe_3O_4-ACLM. The thermodynamic investigation revealed the endothermic aspect and spontaneity of the adsorption process. Using the Langmuir model, the maximum adsorption capacity of the Fe_3O_4-ACLM for the removal of the CIP molecules was 178.8 mg/g, a higher value than for a few adsorbents employed earlier in CIP elimination. Therefore, it was concluded that Fe_3O_4-ACLM was a suitable substitute for other adsorbents in the removal of CIP from aqueous solutions.

Acknowledgements The authors express their gratitude to Dr. Mahdavi for valuable assistance in adsorbent analysis. The authors also extend their thankfulness to the Zahedan University of Medical Sciences for financially supporting this study. Thanks are also due to the Al-Mustaqbal University College for the support offered toward completion of this study.

Author contribution The conception and design of the study are the result of the contributions of all the authors. Murat Yilmaz and Tariq J. Al-Musawi prepared the material, collected the data, and performed the analyses. Davoud Balarak and Marziyeh Baniasadi were responsible for writing the first draft of the manuscript. All the authors provided their comments on the earlier versions of the manuscript. The final manuscript was read and approved by all the authors.

Funding The Zahedan University of Medical Sciences, Zahedan-Iran (code: 10567) has supported the present study.

Data availability In order to request the datasets utilized and analyzed in the present study, the corresponding author may be contacted.

Declarations

Conflict of interests The authors declare no conflict of interest.

References

1. Khodadadi M, Panahi AH, Al-Musawi T, Ehrampoush MH, Mahvi AH (2019) J Water Process Eng 32:100943
2. Balarak D, Azarpira H, Mostafapour FK (2016) Study of the adsorption mechanisms of cephalexin on to azolla filiculoides. Pharm Chem 8:114–121
3. Doroudi Z, Sarvestani MR (2020) Boron nitride nanocone as an adsorbent and senor for Ampicillin: a computational study. Chem Rev Lett 3:110–116
4. Nairi V, Medda L, Monduzzi M, Salis A (2017) Adsorption and release of ampicillin antibiotic from ordered mesoporous silica. J Colloid Interface Sci 497:217–225
5. Balarak D, Mostafapour FK, Bazrafshan E, Saleh TA (2017) Studies on the adsorption amoxicillin on multi-wall carbon nanotubes. Water Sci Technol 75:1599–1606
6. Ji LG, Chen W, Duan L, Zhu D (2009) Mechanisms for strong adsorption of tetracycline to carbon nanotubes: a comparative study using activated carbon and graphite as adsorbents. Environ Sci Technol 43:2322–2327
7. Wang J, Zhuan R (2020) Degradation of antibiotics by advanced oxidation processes: An overview. Sci. Total Environ 701:135023
8. Wang J, Wang S (2018) Microbial degradation of sulfamethoxazole in the environment. Appl Microbiol Biotechnol 102(8):3573–3582
9. Igwegbe CA, Oba SN, Aniagor CO, Adeniyi AG, Ighalo JO (2021) Adsorption of ciprofloxacin from water: a comprehensive review. J Ind Eng Chem 93:57–77
10. Carabineiro SAC, Thavorn-amornsri T, Pereira MFR, Figueiredo JL (2012) Comparison between activated carbon, carbon xerogel and carbon nanotubes for the adsorption of the antibiotic ciprofloxacin. Catal Today 186:29–34
11. Li S, Zhang X, Huang Y (2017) Zeolitic imidazolate framework-8 derived nanoporous carbon as an effective and recyclable adsorbent for removal of ciprofloxacin antibiotics from water. J Hazard Mater 321:711–719
12. El-Shafey H, Al-Lawati AS (2012) Al-Sumri, Ciprofloxacin adsorption from aqueous solution onto chemically prepared carbon from date palm leaflets. J Environ Sci 24(9):1579–1586
13. Carvalho CO, Rodrigues DLC, Lima EC, Umpierres CS, Chaguezac DFC, Machado FM (2019) Kinetic, equilibrium, and thermodynamic studies on the adsorption of ciprofloxacin by activated carbon produced from Jerivá (Syagrus romanzoffiana). Environ Sci Pollut Res Int 26:4690–4702
14. Danalıoğlu ST, Bayazit SS, Kuyumcu OK, Salam MA (2017) Efficient removal of antibiotics by a novel magnetic adsorbent: magnetic activated carbon/chitosan (MACC) nanocomposite. J Mol Liq 240:589–596
15. Wang J, Tang J (2021) Fe-based Fenton-like catalysts for water treatment: preparation, characterization and modification. Chemosphere. 276:130177
16. Wang J, Chen H (2020) Catalytic ozonation for water and wastewater treatment: recent advances and perspective. Sci Total Environ. 20:135249
17. Liu Y, Zhao Y, Wang J (2021) Fenton/Fenton-like processes with in-situ production of hydrogen peroxide/hydroxyl radical for degradation of emerging contaminants: advances and prospects. J Hazard Mater. 404:124191
18. Patraa C, Suganyaa E, Sivaprakasama S, Krishnamoorthy G, Narayanasamy S (2021) A detailed insight on fabricated porous chitosan in eliminating synthetic anionic dyes from single and multi-adsorptive systems with related studies. Chemosphere. 281:130706
19. Chandrasekaran A, Patra C, Narayanasamy S, Subbiah S (2020) Environ. Res. 188:109825
20. Zhu X, Tsang DCW, Chen F, Li S, Yang X (2015) Ciprofloxacin adsorption on graphene and granular activated carbon: kinetics, isotherms, and effects of solution chemistry. Environ Technol 36:3094–3102
21. Wang F, Yang B, Wang H, Song Q, Tan F, Cao Y (2016) Removal of ciprofloxacin from aqueous solution by a magnetic chitosan grafted graphene oxide composite. J Mol Liq 222:188–194
22. Falyouna O, Maamoun I, Bensaida K, Tahara A, Sugihara Y, Eljamal O (2022) Encapsulation of iron nanoparticles with magnesium hydroxide shell for remarkable removal of ciprofloxacin from contaminated water. J Colloid Interface Sci 605:813–827
23. Ciğeroğlu Z (2021) "Preparation of ZnO/BaTiO3 adsorbent using Elaeagnus Angustifolia L. leaf extract and its evaluation for ciprofloxacin removal from aqueous solutions: an optimization study." Biomass Convers. Biorefin 22:1–11
24. Wang J, Guo X (2020) Adsorption isotherm models: classification, physical meaning, application and solving method. Chemosphere. 258:127279
25. Azarpira H, Mahdavi Y, Khaleghi O (2016) Thermodynamic studies on the removal of metronidazole antibiotic by multi-walled carbon nanotubes. Pharm Lett 8(11):107–124
26. Al-Musawi TJ, Mahvi AH, Khatibi AD (2021) Effective adsorption of ciprofloxacin antibiotic using powdered activated carbon magnetized by iron(III) oxide magnetic nanoparticles. J Porous Mater 28:835–852
27. Patra C, Shahnaz T, Subbiah S, Narayanasamy S (2020) Comparative assessment of raw and acid-activated preparations of novel Pongamia pinnata shells for adsorption of hexavalent chromium from simulated wastewater. Environ Sci Pollut Res 27:14836–14851
28. Patra C, Medisetti MN, Pakshirajan K, Narayanasamy S (2019) Assessment of raw, acid-modified and chelated biomass for sequestration of hexavalent chromium from aqueous solution using Sterculia villosa Roxb. Shells Environ Sci Pollut Res 2019(26):23625–23637
29. Khatibi AD, Mahvi AH, Mengelizadeh N (2021) Adsorption-desorption of tetracycline onto molecularly imprinted polymer: isotherm, kinetics, and thermodynamics studies. Desal Water Treat 230:240–251
30. Nasseh N, Al-Musawi TJ, Miri MR, Rodriguez-Couto S, Panahi AH (2020) A comprehensive study on the application of FeNi3@SiO2@ZnO magnetic nanocomposites as a novel photo-catalyst

for degradation of tamoxifen in the presence of simulated sunlight. Environ. Pollut. 261:114127
31. Mohseni-Bandpi A, Al-Musawi TJ, Ghahramani E, Zarrabi M, Mohebi S, Vahed SA (2016) Improvement of zeolite adsorption capacity for cephalexin by coating with magnetic Fe_3O_4 nanoparticles. J Mol Liq 218:615–624
32. Vecchio PD, Haro NK, Souza FS, Marcilio NR, Feris LS (2019) Ampicillin removal by adsorption onto activated carbon: kinetics, equilibrium and thermodynamics. Water Sci Technol 79(10):2013–2021
33. Mohammed AA, Brouers F, Isra'a Sadi S, Al-Musawi TJ. (2018) Role of Fe_3O_4 magnetite nanoparticles used to coat bentonite in zinc(II) ions sequestration. Environ Nanotechnol Monit Manag 10:17–27
34. Balarak D, Mahvi AH, Shahbaksh S, Wahab MA, Abdala A (2021) Adsorptive removal of azithromycin antibiotic from aqueous solution by azolla filiculoides-based activated porous carbon. Nanomaterials 11(12):3281
35. Popoola LT (2019) Tetracycline and sulfamethoxazole adsorption onto nanomagnetic walnut shell-rice husk: isotherm, kinetic, mechanistic and thermodynamic studies. Int J Environ Anal Chem 100:1–23
36. Al-Musawi TJ, Mengelizadeh N, Al Rawi O, Balarak D (2021) Capacity and modeling of acid blue 113 dye adsorption onto chitosan magnetized by Fe2O3 nanoparticles. J Polym Environ. https://doi.org/10.1007/s10924-021-02200-8
37. Balarak D, Baniasadi M, Lee SM, Shim MJ (2021) Ciprofloxacin adsorption onto Azolla filiculoides activated carbon from aqueous solutions. Desal Water Treat 218:444–453
38. Mahvi AH, Mostafapour FK (2018) Biosorption of tetracycline from aqueous solution by Azolla Filiculoides: Equlibrium kinetic and thermodynamic studies. Fresenius Environ Bull 27:5759–5767
39. Diyanati R, Yazdani J (2013) EEffect of sorbitol on phenol removal rate by lemna minor. J Mazand Uni Med Sci 22:58–65
40. Dyanati-Tilaki RA, Yousefi Z, Yazdani-Cherati J (2013) The ability of azollaand lemna minor biomassfor adsorption of phenol fromaqueous solutions. J Mazand Uni Med Sci 23:140–146
41. Liu H, Liu W, Zhang J, Zhang C, Ren L, Li Y (2011) Removal of cephalexin from aqueous solution by original and Cu(II)/Fe(III) impregnated activated carbons developed from lotus stalks kinetics and equilibrium studies. J Hazard Mater 185:1528–1535
42. Xu L, Pan J, Dai J, Li X, Hang H, Cao Z, Yan Y (2012) Preparation of thermal-responsive magnetic molecularly imprinted polymers for selective removal of antibiotics from aqueous solution. J Hazard Mater 233–234:48–56
43. Peterson JW, Petrasky LJ, Seymourc MD (2012) Adsorption and breakdown of penicillin antibiotic in the presence of titanium oxide nanoparticles in water. Chemosphere 87:911–917
44. Meshkinain A, Davoud B, Y. Nastaran Y. (2021) Optimization of nickel oxide nanoparticle synthesis through the sol-gel method for adsorption of Penicillin G. Res J Chem Environ 25(3):31–36
45. Ahmadi S, Banach A, Mostafapour FK (2017) Study survey of cupric oxide nanoparticles in removal efficiency of ciprofloxacin antibiotic from aqueous solution: adsorption isotherm study. Desalin Water Treat 89:297–303
46. Balarak D, Mahvi AH, Shim MJ, Lee SM (2021) Adsorption of ciprofloxacin from aqueous solution onto synthesized NiO: isotherm, kinetic and thermodynamic studies. Desalin Water Treat 212:390–400
47. Adekola FA, Adegoke HI, AdebayoGB ALO (2016) Batch sorption of ciprofloxacin on kaolinitic clay and nhematite composite: equilibrium and thermodynamics studies. Mor J Chem 4:384–424
48. Sousa DN, Oliveira AR, Filho JFC, Dantas TCM, Santos AGD, Caldeira VPS, Geraldo EL (2018) Ciprofloxacin adsorption on ZnO supported on SBA-15. Water Air Soil Pollut 229:1–12
49. Yin D, Xu Z, Shi J, Shen L, He Z (2017) Adsorption characteristics of ciprofloxacin on the schorl: kinetics, thermodynamics, effect of metal ion and mechanisms. J Water Reuse Desal 8:350–359
50. Wang L, Chen G, Ling C, Zhang J, Szerlag K (2017) Adsorption of ciprofloxacin on to bamboo charcoal: effects of pH, salinity, cations, and phosphate. Environ Prog Sustain 36:1108–1115
51. Jiang WT, Chang PH, Wang YS, Tsai Y, Jean JS, Li Z, Krukowski K (2013) Removal of ciprofloxacin from water by birnessite. J Hazard Mater 250:362–369
52. Fakhri A, Adami S (2014) Adsorption and thermodynamic study of Cephalosporins antibiotics from aqueous solution onto MgO nanoparticles. J Taiwan Inst Chem Eng 45:1001–1006
53. Sharma N, Dehiman N (2017) Kinetic and thermodynamic studies for ciprofloxacin hydrochloride adsorption from aqueous solution on CuO nanoparticles. Int J Chem Tech Res 10:098–106
54. Ahmed MJ, Theydan SK (2014) Fluoroquinolones antibiotics adsorption onto microporous activated carbon from lignocellulosic biomass by microwave pyrolysis. J Taiwan Inst Chem Eng 45:219–226
55. Sharma G, Kumar A, Dhiman P, AlGarni TS, Naushad M, Stadler FJ (2022) Controlled synthesis of porous Zn/Fe based layered double hydroxides: Synthesis mechanism, and ciprofloxacin adsorption. Sep. Purif. Technol 278:119481
56. Patra C, Gupta R, Bedadeep D, Narayanasamy S (2020) Surface treated acid-activated carbon for adsorption of anionic azo dyes from single and binary adsorptive systems: A detail insight. Environ. Pollut. 266:115102
57. Baccar R, Sarrà M, Bouzid J, Feki M, Blánquez P (2012) Removal of pharmaceutical com-pounds by activated carbon prepared from agricultural by-product. Chem Eng J 211:310–317
58. Chih-Jen W, Zhaohui L, Wei-The J (2011) Adsorption of ciprofloxacin on 2:1 dioctahedral clay minerals. Appl Clay Sci 53:723–728
59. Fakhri A, Rashidi S, Asif M, Tyagi I, Agarwal S, Gupta VK (2016) Dynamic adsorption behavior and mechanism of Cefotaxime, Cefradine and Cefazolin antibiotics on CdS-MWCNT nanocomposites. J Mol Liq 215:269–275
60. Behera SK, Oh SY, Park HS (2012) Sorptive removal of ibuprofen from water using selected soil minerals and activated carbon. Int J Environ Sci Technol 9:85–94
61. Rahman N, Varshney P (2020) Assessment of ampicillin removal efficiency from aqueous solution by polydopamine/zirconium(IV) iodate: optimization by response surface methodology. RSC Adv 10:20322–20337
62. Chitongo R, Opeolu BO, Olatunji OS (2019) Abatement of Amoxicillin, Ampicillin, and Chloramphenicol from aqueous solutions using activated carbon prepared from grape slurry. Clean: Soil, Air, Water 47:1800077
63 Al-Musawi TJ, Mengelizadeh N, Taghavi M (2021) Biomass Conv. Bioref. 3:1–13. https://doi.org/10.1007/s13399-021-01962-4
64. Balarak D, Taheri Z, Shim MJ, Lee SM, Jeon C (2021) Adsorption kinetics and thermodynamics and equilibrium of ibuprofen from aqueous solutions by activated carbon prepared from Lemna minor. Desal Water Treat 215:183–193